European Journal of Mechanics B/Fluids 48 (2014) 59–74

Contents lists available at ScienceDirect

European Journal of Mechanics B/Fluids

journal homepage: www.elsevier.com/locate/ejmflu

Investigation of aerodynamic characteristics of rarefied flow around NACA 0012 airfoil using DSMC and NS solvers

Ahmad Shoja-Sani [a], Ehsan Roohi [a,*], Mohsen Kahrom [a], Stefan Stefanov [b]

[a] High Performance Computing (HPC) Laboratory, Department of Mechanical Engineering, Faculty of Engineering, Ferdowsi University of Mashhad, P.O. Box 91775-1111, Mashhad, Iran

[b] Institute of Mechanics, Bulgarian Academy of Science, Acad. G. Bontchev str., 1113, Sofia, Bulgaria

HIGHLIGHTS

- Simulation of the subsonic/supersonic flows around an airfoil at rarefied conditions.
- Investigation of aerodynamics characteristics of small scale airfoil.
- Investigation of continuum approach suitability in rarefied conditions.
- Prediction of force coefficients and drag polar in rarefied conditions.

ARTICLE INFO

Article history:
Received 20 June 2013
Received in revised form
16 February 2014
Accepted 22 April 2014
Available online 30 April 2014

Keywords:
NACA 0012 airfoil
Rarefied flow
DSMC
Slip/jump boundary conditions
OpenFOAM

ABSTRACT

In this study, rarefied supersonic and subsonic gas flow around a NACA 0012 airfoil is simulated using both continuum and particle approaches. Navier–Stokes equations subject to the first order slip/jump boundary conditions are solved under the framework of OpenFOAM package. The DSMC solver of the package, i.e., dsmcFoam, has been improved to include a newly presented "simplified Bernoulli trial (SBT)" scheme for inter-molecular collision modeling. The use of SBT collision model permits to obtain accurate results using a much lower number of simulator particles. We considered flow at different angles of attacks and Knudsen numbers at both the subsonic and supersonic regimes. The computed density and surface pressure distributions are compared with the experimental and numerical data and suitable accuracy was observed. We investigate variations of the lift and drag coefficients with the Knudsen number and angle of attack. At low Kn number in supersonic regime, our results for lift coefficient agree well with the linearized theory; however, the deviation starts as soon as the angle of attack goes beyond 15° or shock wave forms above the airfoil. Along with this, we have observed that drag coefficient increases with the Kn number increasing. We also investigated the effect of Kn number on the leading edge shock position and structure, drag polar (C_L/C_D), and slip velocity over the airfoil.

© 2014 Elsevier Masson SAS. All rights reserved.

1. Introduction

There is great interest in the development of very small aircraft, such as the micro air vehicle (MAV), for a wide range of missions. Most of the current MAV's are scaled-down versions of conventional aircraft. MAV's experience low Reynolds number flows characterized by chord lengths of a few centimeters; therefore, fundamental studies are required to understand the aerodynamic features of MAV's. Once the characteristic scales of a device are sufficiently small, the non-equilibrium, rarefied flow phenomena become dominant. The key parameter describing the degree of gas rarefaction is the Knudsen number defined as:

$$\mathrm{Kn} = \lambda/L. \tag{1}$$

It is the ratio of the mean free path of the gas molecules, λ, to the characteristic length of the geometry, L. Based on the variable hard sphere (VHS) molecular model, the mean free path is related to the gas viscosity as follows:

$$\lambda = \frac{2}{15}(5-2\omega)(7-2\omega)\sqrt{\frac{m}{2\pi kT}}\left(\frac{\mu_g}{\rho}\right) \tag{2}$$

where μ_g is the gas viscosity and ω is the macroscopic viscosity–temperature exponent. Based on the Knudsen number, the flow is classified into four different regimes [1]: continuum, slip flow,

* Corresponding author. Tel.: +98 511 8805136; fax: +98 511 8763304.
E-mail address: e.roohi@ferdowsi.um.ac.ir (E. Roohi).

http://dx.doi.org/10.1016/j.euromechflu.2014.04.008
0997-7546/© 2014 Elsevier Masson SAS. All rights reserved.

transition and free molecular regimes. For the Kn < 0.001, i.e., continuum regime, the NS equation with the standard no-slip boundary condition can be employed to describe the flow behavior. In slip flow regime, $0.001 < \mathrm{Kn} < 0.1$, the NS equations should be accompanied with the velocity slip and temperature jump boundary conditions over the walls [2,3]. In the transition regime, $0.1 < \mathrm{Kn} < 10$, the core flow gradually departs from the equilibrium and the NS equations are no longer valid. Finally, the flow is considered as free molecular as it goes beyond the limit of $\mathrm{Kn} > 10$.

Direct simulation Monte Carlo (DSMC) is a standard tool for simulating rarefied flow through all rarefaction regimes from the slip to the free molecular one. In this approach, the fluid is modeled as a set of moving particles interacting through binary collisions. The DSMC method is known as one of the most successful particle-based methods in analyzing the rarefied gas flows. The main feature of the DSMC method, originally proposed by Bird [4], is decoupling particle's motion and binary collisions within the grid cells in each time step.

The aim of the current study is to simulate rarefied flow field around a NACA 0012 airfoil using the NS and DSMC solvers. We selected NACA 0012 airfoil because it is a very conventional airfoil whose experimental data is available even in the rarefied flow regime, i.e., Allegre et al. [5,6] performed experimental studies on the NACA 0012 airfoil in sub and supersonic rarefied gas flow in the slip regime and investigated the effect of velocity slip on the flow field. They presented experimental results for density and velocity flow field at three angles of attack. Allegre [5] and Hasse [7] reported that there is a significant difference between the no-slip Navier–Stokes and experimental density field. A further investigation at Mach 2.0 and zero angle of attack showed that this difference may be considerably reduced when the wall slip velocity and temperature jump boundary conditions were included in the calculations [6,8]. Fan et al. [9] studied computational flow field around NACA 0012 airfoil in Mach 2 and $\mathrm{Kn} = 0.026$ in the slip flow and sub/supersonic regimes. They used low-noise information preservation (IP) technique to simulate low speed flows more efficiently. Sun and Boyd [10] studied subsonic gas flow over a flat-plate airfoil at very-low Reynolds number in order to investigate the aerodynamic issues related to micro air vehicle design and performance. They showed that low Reynolds number flows are viscous and compressible and rarefaction effects increase when the Reynolds number decreases. Zuppardi et al. [11] performed a preliminary analysis about the possibility of aerodynamic control of the space vehicles by the deflection of a trailing edge flap. This analysis has been carried out in terms of the lift and drag forces and pitching moment at the altitude of 70 km. The flow field has been solved by both of a 2D DSMC code (DS2V) and computational fluid dynamic code (H3NS).

In this work, we study rarefied gas flows around a NACA 0012 airfoil at Mach numbers of 2 and 0.8 and over a wide range of angle of attack. Our cases are simulated in four Kn numbers, based on the chord length of the airfoil, i.e., $\mathrm{Kn} = 0.014$, 0.026 and $\mathrm{Kn} = 0.1$ in the slip flow regime and $\mathrm{Kn} = 0.26$ in the early transition regime. There are available experimental data in the literature to compare in these Mach numbers and two angles of attacks, i.e., 0° and 10°, and in the slip flow regime for density and velocity flow fields [5,6]. The main focus of this study is to report the effects of increasing of the Knudsen number on the force coefficients, i.e., aerodynamics characteristics at rarefied conditions, and to provide physical descriptions on the flow dependency on the rarefaction state at different Mach number regimes. Our literature survey shows that previous works [5–11] did not focus on the aerodynamic characteristics of the rarefied flows over airfoils at both of sub and supersonic regimes. This work should be considered as the continuation of the authors' previous researches in rarefied gas dynamics [12–15]. It should be noted that supersonic speed flight is currently possible for unmanned aerial vehicles, and the current research on high speed/high Knudsen number flight of MAV's could be considered as a research base for future perspective of small scale vehicle flight.

2. Numerical method

2.1. Continuum approach

The compressible NS equations can be derived from the Chapman–Enskog expansion of the Boltzmann equation. These equations, conservation of mass, momentum and total energy, are written as [16]

$$\frac{\partial \rho}{\partial t} + \nabla \cdot (\rho \boldsymbol{V}) = 0 \tag{3}$$

$$\frac{\partial (\rho \boldsymbol{V})}{\partial t} + \nabla \cdot (\boldsymbol{V}(\rho \boldsymbol{V})) + \nabla p + \nabla \cdot \boldsymbol{\tau} = 0 \tag{4}$$

$$\frac{\partial (\rho E)}{\partial t} + \nabla \cdot (\boldsymbol{V}(\rho E)) + \nabla \cdot (\boldsymbol{V} p) + \nabla \cdot (\boldsymbol{\tau} \cdot \boldsymbol{V}) + \nabla \cdot \boldsymbol{q} = 0, \tag{5}$$

where ρ is the fluid density, p is the pressure, $E = e + |\boldsymbol{V}^2|/2$ is the total energy, e is the internal energy per unit mass, $\mathbf{q}$ is the conductive heat transfer, and $\boldsymbol{\tau}$ is the shear stress tensor, which is related to the velocity field via the Newton law as follows:

$$\boldsymbol{\tau} = -2\mu \,\mathrm{dev}(\boldsymbol{D}) \tag{6}$$

$$\mathbf{D} = 0.5[\nabla \boldsymbol{V} + (\nabla \boldsymbol{V})^T], \tag{7}$$

where μ is the dynamic viscosity, and "dev" denotes the deviatoric of a tensor, i.e., $\mathbf{D} - (1/3)\mathrm{tr}(\mathbf{D})\boldsymbol{I}$, where $\boldsymbol{I}$ is the unit tensor and tr is the trace of a tensor. Here, we considered a calorically perfect gas for all simulations. So, $p = \rho RT$ and $e = c_v T$, where c_v is the specific heat at constant volume and R is the gas constant. Due to the low temperature of the flow field, the translational and rotational temperatures are almost equal and there is no need of adding of governing equations for rotational and vibrational energies. Due to the same reason, air could be considered as a mixture of nitrogen and oxygen, therefore, one set of governing equation is employed for the working fluid.

In the current work, the continuum approach solves the NS equations with slip/jump boundary conditions on the airfoil surface using the "rhoCentralFoam" solver of the OpenFOAM [17]. RhoCentralFoam is an explicit, collocated finite volume, density-based solver to simulate viscous compressible flows [18]. In the finite volume method, the governing equations are integrated over all cell volumes. The divergence and gradient terms are then replaced with integrals over the cell surface using the Gauss's theorem. These integrations require the flux evaluation over the cell faces, which are subsequently approximated using suitable interpolations of the cell center values. In "rhoCentralFoam", the required interpolations are performed using the second-order semi-discrete, non-staggered schemes of Kurganov and Tadmor (KT) [19] and Kurganov, Noelle, and Petrova (KNP) [20]. This solver is an explicit solver, i.e., all new solutions at the current time step are calculated explicitly from the known magnitudes of the previous time step. Since the explicit approaches are faced with a time step limit, a sequential operator splitting approach is employed to consider the diffusive terms as suitable implicit corrections of an approximate inviscid solution.

2.2. Slip/jump boundary conditions

We used the Maxwell–Smoluchowski slip/jump boundary conditions allowing for the presence of an imperfect momentum and energy accommodation over the surface as follows [2]:

$$\mathbf{V}_g - \mathbf{V}_w = -\frac{2-\sigma_u}{\sigma_u}\lambda\nabla_n(\mathbf{S}\cdot\mathbf{V}) - \frac{2-\sigma_u}{\sigma_u}\frac{\lambda}{\mu}\mathbf{S}\cdot\left(\mathbf{n}\cdot\prod_{mc}\right) - \frac{3}{4}\frac{\mu}{\rho}\frac{\mathbf{S}\cdot\nabla T}{T} \tag{8}$$

$$T_g - T_w = -\frac{2-\sigma_T}{\sigma_T}\frac{2\gamma}{(\gamma+1)\,\mathrm{Pr}}\lambda\nabla_n T \tag{9}$$

where $\boldsymbol{n}$ represents the unit normal vector to the surface and μ is the dynamic viscosity. Additionally, the subscripts g and w refer to gas adjacent to the wall and the wall, respectively. σ_u and σ_T are the tangential momentum and thermal accommodation coefficients, respectively. γ is the specific heat ratio and Pr is the Prandtl number. The tensor $\mathbf{S} = \mathbf{I} - \mathbf{nn}$, considering $\mathbf{I}$ as the identity tensor, removes the normal components of any non-scalar field. $\prod_{mc}$ is expressed as

$$\mathbf{\Pi}_{mc} = \mu(\nabla\mathbf{V})^T - (2/3)\mathbf{I}_{tr}(\nabla\mathbf{V}), \tag{10}$$

where subscript tr denotes the trace. To be consistent with DSMC simulations presented here, we consider both accommodation coefficients σ_u and σ_T equal to one. It should be noted that alternative slip/jump boundary conditions with higher accuracy were also derived, i.e., see Ref. [21]; however, as we will show in this paper, standard BC's employed in OpenFOAM could provide nearly accurate results for supersonic flow in the slip regime.

2.3. Particle approach

The DSMC method is the dominant numerical technique for solving rarefied flows [4]. Here, we used the dsmcFoam as our DSMC solver [22]. The dsmcFoam has been developed within the framework of the open source CFD package of OpenFOAM. It is a parallel DSMC solver which can model arbitrary geometries and arbitrary number of gas species. It uses the variable hard sphere (VHS) collision model and the Larsen–Borgnakke internal energy redistribution model to simulate the inter-molecular collisions. We set the reference temperature and viscosity as 273 K and 1.79×10^{-5} Pa · s and assumed air stream as a gas mixture of oxygen with viscosity–temperature index of $\omega = 0.77$ and nitrogen with $\omega = 0.74$. We modified the original dsmcFoam solver to use "simplified Bernoulli trial (SBT)" scheme [23] for selection of the collision pairs.

Briefly, the dsmcFoam sub-algorithms can be categorized in two major parts

(1) Particle tracking in unstructured, arbitrary, polyhedral meshes: The particle tracking algorithm of dsmcFoam has been inherited from the algorithms originally written for the molecular dynamics solver of the OpenFOAM [24].
(2) Distributing particles in arbitrary cell volumes for initial random configuration of the particles, and uniformly allocating incoming particles from the free-stream boundaries: in fact, to distribute particles in the cell volume and free-stream faces, each cell/face is first divided into a number of tetrahedrals/triangles. Selecting a random number, particles are positioned in the corresponding tetrahedral/triangle whose volume/area fraction is larger than the random number.

The macroscopic flow properties are sampled in each cell using the molecular velocities as soon as the flow reaches the steady-state condition. The sampling process is continued long after reaching the steady solution to suppress the inherent statistical scatters which show up in the DSMC method. In such extent, wall pressure, shear stress, normal and axial force coefficients, lift and drag coefficients and slip velocity are obtained from [25,26]

$$p_w = \frac{1}{t_s A}\sum_{j=1}^{N_s} m(V^r_{n,j} - V^i_{n,j}), \qquad C_P = \frac{P_w - P_\infty}{1/2\rho_\infty U_\infty^2} \tag{11}$$

$$\tau_w = \frac{1}{t_s A}\sum_{j=1}^{N_s} m(V^r_{t,j} - V^i_{t,j}), \qquad C_f = \frac{\tau_w}{1/2\rho_\infty U_\infty^2} \tag{12}$$

$$C_n = \frac{1}{c}\left[\int_0^c (C_{p,l} - C_{p,u})dx + \int_0^c \left(C_{f,u}\frac{dy_u}{dx} - C_{f,l}\frac{dy_l}{dx}\right)dx\right] \tag{13}$$

$$C_a = \frac{1}{c}\left[\int_0^c \left(C_{p,u}\frac{dy_u}{dx} - C_{p,l}\frac{dy_l}{dx}\right)dx + \int_0^c (C_{f,u} - C_{f,l})dx\right] \tag{14}$$

$$c_l = c_n\cos(\alpha) + c_a\sin(\alpha) \tag{15}$$

$$c_d = c_a\cos(\alpha) - c_n\sin(\alpha) \tag{16}$$

$$u_{slip} = \frac{\sum\left(\frac{m}{|v_p|}u_p\right)}{\sum\left(\frac{m}{|v_p|}\right)} \tag{17}$$

where n and t indicate normal and tangential components, r and i refer to reflected and incident particles, t_s is the sampling time, A is the area of the surface element, m is the particle mass, N_s is the number of samples, u and l refer to upper and lower surfaces of the airfoil, c is the chord of the airfoil, α is the angle of attack (AoA), p refers to particle, $|v_p|$ is the absolute value of the normal velocity, and u_p is the axial component of the particle velocity.

2.4. SBT scheme

One of the important parts of any DSMC code is the selection of collision pair. At the homogeneous gas stream, the probability of collision between two particles is proportional to the relative velocity of two particles multiplied by the collision cross section of them [26]. The selection of collision pairs in the original dsmcFoam is based on the no time counter (NTC) method. In this method, the number of particle pairs that should be checked for collision is:

$$Num_{Collision-Max} = \frac{N(N-1)EN(\sigma_T C_r)_{\max}\Delta t}{2V_c}, \tag{18}$$

where N is number of simulated particles, EN presents the ratio of the number of real molecules to the simulated particles (N). σ_T, C_r and V_c are molecular collision cross section, relative velocity of the two particles and the volume of the cell, respectively. Then, each pair (i, j), $1 \le i < j \le N$, chosen randomly from the particle subset N, is checked for a collision with the probability

$$p_{ij} = \frac{(\sigma_T C_r)_{ij}}{(\sigma_T C_r)_{max}}, \tag{19}$$

where $(\sigma_T C_r)_{ij}$ is the molecular collision cross section multiplied by the relative velocity for the pair (i, j). NTC approach is an efficient method for simulating the collision between particles, but at low Knudsen number or when a large number of grid cells is used, it requires a very large number of particles, which subsequently increases the computational costs.

In this work, we use "Simplified Bernoulli Trail", introduced first by Stefanov [23], to reduce the computational cost and memory in comparison with the NTC method. The method provides a good possibility to do simulations with a much lower number of particles per cell, even at low Knudsen number [27]. In this approach, similar to NTC, first the particles in each cell should be arranged in order to form a list of numbered particles as $1, \ldots, N$. The first particle of collision pair (i, j), say i, is selected in sequence from the particle list, i.e., $i = 1, \ldots, N-1$. The second particle, say j, is then selected randomly among $k = N - i$ particles taking their place in the list after particle i.

$$j = (i+1) + int(k \times rnd), \tag{20}$$

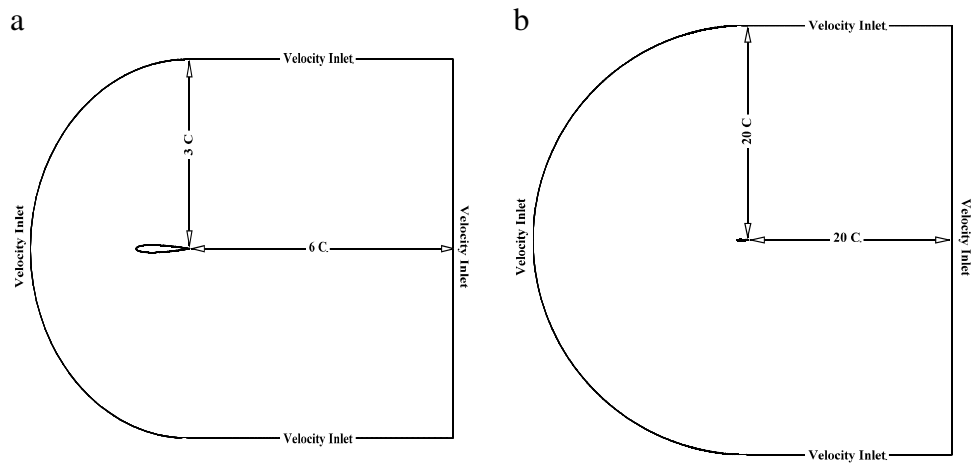

Fig. 1. The computational domain configuration along with employed boundary conditions (a) supersonic computational domain (b) subsonic computational domain.

where *rnd* refers to a random number between 0 and 1. Then, each pair is checked for possible collision with the probability

$$p_{ij} = kEN\Delta t(\sigma_T C_r)_{ij}/V_c. \tag{21}$$

It should be noted that the Δt should be adjusted so that p_{ij} does not exceed unity, say

$$prob\left\{p_{ij} \geq 1\right\} \rightarrow 0. \tag{22}$$

The detailed theoretical background of this scheme is described in Ref. [23].

3. Results and discussions

3.1. Test description

Air flow around the NACA 0012 airfoil is considered. The profile of this airfoil is obtained using the following formula:

$$y = 0.6\left(0.2969\left(\frac{x}{c}\right)^{\frac{1}{2}} - 0.126\left(\frac{x}{c}\right) - 0.3537\left(\frac{x}{c}\right)^2 + 0.2843\left(\frac{x}{c}\right)^3 - 0.1015\left(\frac{x}{c}\right)^4\right) \tag{23}$$

where c is the chord length, x is the position along the chord (from 0 to c), y is the half thickness of the airfoil at the given value of x (centerline to surface). The chord length is considered as 4 cm. The airfoil is located in an air stream with $V_\infty = 509$ m/s (Mach = 2) and $T = 161$ K at supersonic regime and $V_\infty = 257$ m/s (Mach = 0.8) and $T = 257$ K at subsonic regime. The airfoil surface temperature is $T_s = 290$ K, which is equal to the stagnation temperature. The air is considered as a mixture of 21% oxygen and 79% nitrogen. The computational domain consists of structured grids and rectangular cells. The grid conforms to the airfoil surface and extends to a semi-circular region on the upstream boundary with a radius equal to 3 chords and a rectangular backward boundary with 6 chord length. In subsonic cases, we use a quite larger domain with around 20 chord length size at both of upstream and downstream of the airfoil to remove the effect of the airfoil disturbances on the imposed boundary conditions. At all outer edges of the computational grid, we apply free stream conditions using velocity inlet boundary condition. Fig. 1 shows the computational domain with employed boundary conditions for the sub/supersonic flow regimes.

Fig. 2 shows the grid at the leading edge of the airfoil. DSMC time step was chosen as 3×10^{-7} s. In a typical test case, our sample size was about 600,000 in each cell. For all of our NS simulations, the Courant number was set equal to 0.3.

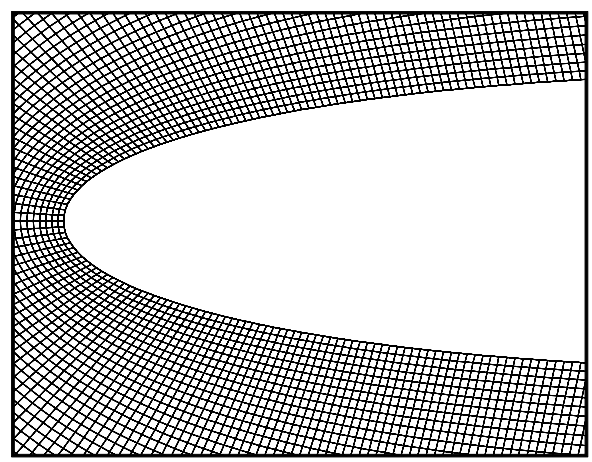

Fig. 2. A zoomed view of the grid used on the leading edge at $\alpha = 0°$.

3.1.1. Particle number, grid size and time step independency study

Since the DSMC calculation is sensitive to the number of particles, a particle number independency investigation was carried out using six different sets of number of particles per cell: 1, 2, 4, 8, 16 and 32 simulated particles per cell at the Kn number of 0.26 and 45° of angle of attack. The key benefit of using the SBT collision scheme is its ability to provide accurate solutions using even few particles per cell [23,27]. This is in contrast to the standard collision scheme such as (NTC) available in the original version of dsmcFoam. Fig. 3(a) shows the pressure coefficient distribution (C_p) on the upper and lower surfaces of the airfoil. It is observed that C_p is almost the same for all cases, even for 1 particle per cell case. This illustrates independency of pressure coefficient from the number of simulated particles. Fig. 3(b) shows the normalized slip velocity (V_s/V_∞) on the airfoil surface. Slip velocity; however, is more sensitive to the number of DSMC particles compared to C_p. We observed that the results obtained using few particles per cell show some fluctuations.

Table 1 indicates the lift and drag coefficients for 6 cases considered here. As the table shows, C_L and C_D for 6 cases are approximately the same. This point shows that accurate solution for force coefficients could be obtained using even 2 particles per cell for the considered test case. However, we used 4 particles per cell for the simulation results reported here to decrease the fluctuations in the flow field properties.

For DSMC solution, the grid independency study was also carried out. For grid independency test, four set of cells on the airfoil surface at an angle of attack $\alpha = 45°$ and Kn number equal to 0.26

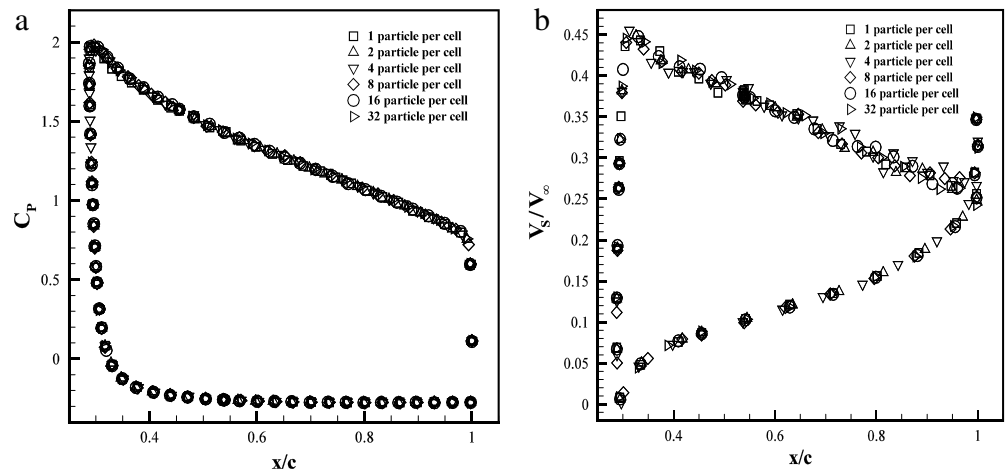

Fig. 3. Particle independency test at Mach = 2, Kn = 0.26 and $\alpha = 45°$ (a) Pressure coefficient distribution, (b) Slip velocity distribution.

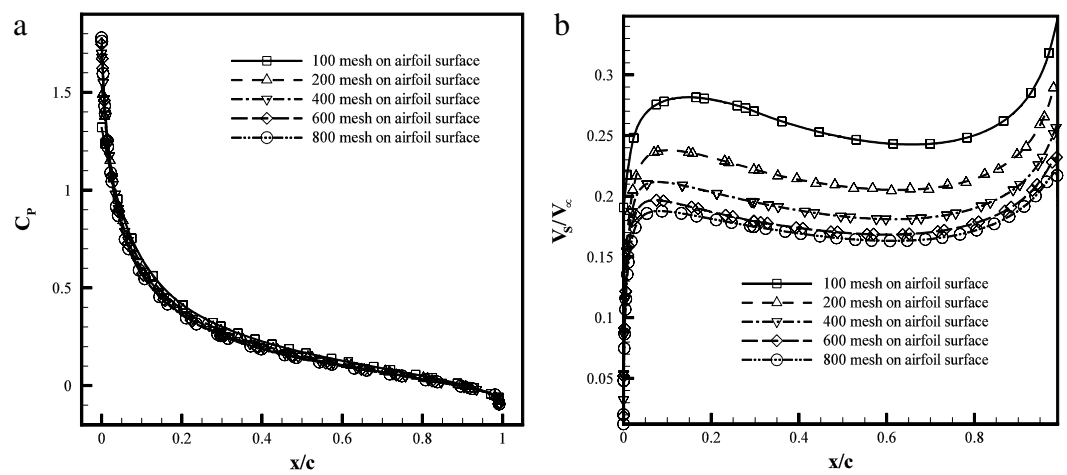

Fig. 4. Grid independency study at Mach = 2, Kn = 0.026 and $\alpha = 0°$ (a) pressure distribution coefficient, (b) slip velocity distribution.

Table 1
Magnitudes of C_L and C_D for different particles per cell tests at Mach = 2, Kn = 0.26 and AoA = 45°.

Number of particles per cell						
	1	2	4	8	16	32
C_L	0.9328	0.9345	0.9351	0.9356	0.9361	0.9359
C_D	1.5069	1.5054	1.5064	1.5068	1.5078	1.5081

Table 2
Magnitudes of C_L and C_D for different grid sizes at Mach = 2, Kn = 0.26 and AoA = 45°.

Number of cells on the airfoil surface, DSMC solution				
	200	400	600	800
C_L	0.9352	0.9347	0.9351	0.9352
C_D	1.5037	1.5050	1.5064	1.5073

was considered: 200, 400, 600 and 800 cells on the surface. In all cases, we used 4 particles per cell. The lift and drag coefficients for grid independency test case are shown in Table 2. The values in the table show that the changes in C_L and C_D are less than 1% when the number of grid increases from 600 up to 800 cells on the airfoil surface. Therefore, we used the 600 cells on the airfoil surface to obtain accurate results with an affordable computational cost.

We also performed domain size and time step independency test for the DSMC solution at the same Kn number and angle of attack. For domain independency test, we increased the size of the domain shown in Fig. 2 by a factor of 2. The C_L and C_D coefficients obtained from the DSMC solution for this domain are 0.9285 and 1.5075, respectively. In comparison with column 3 of Tables 1 and 2, we observe that the change in force coefficients is small, which confirms the suitability of the domain size indicated in Fig. 2. For time step independency, we tested the same test case at Kn = 0.26 and angle of attack of 45° with three different time steps. The results for force coefficients are reported in Table 3. The table shows that the time step of 3×10^{-7} s is proper for our simulations.

Table 3
Magnitudes of C_L and C_D for different time steps at Mach = 2, Kn = 0.26 and AoA = 45°.

Time step ($\times 10^{-7}$) s			
	1	3	6
C_L	0.9352	0.9351	0.9351
C_D	1.5071	1.5064	1.5081

3.1.2. Grid independency study for the NS solver

As NS solutions are sensitive to the grid resolution, it is necessary that we consider the independency of our solution from the number of numerical grids. We performed a grid independency study for our NS solution using five different sets of grids. These contain 100, 200, 400, 600 and 800 grid cells on the airfoil surface. Fig. 4 shows the distribution of pressure coefficient and normalized slip velocity over the airfoil surface. Fig. 4(a) indicates that the

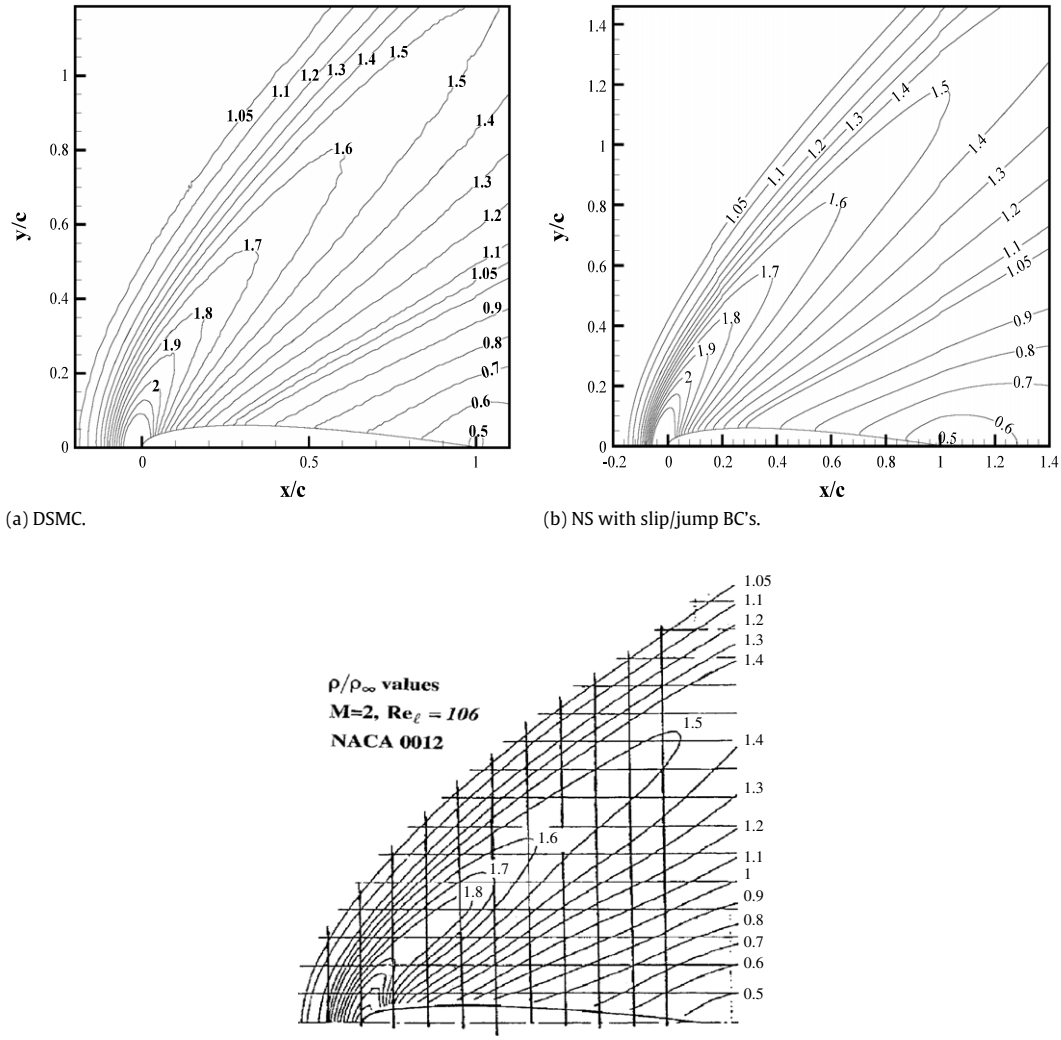

(a) DSMC.

(b) NS with slip/jump BC's.

(c) Experiment [5,6].

Fig. 5. Comparison of the density field from the DSMC and slip/jump NS solution with the experimental data [5,6] at Mach = 2, Kn = 0.026 and $\alpha = 0°$.

Table 4
Magnitudes of C_D on the leading edge of the airfoil at different grid sizes at Mach = 2, Kn = 0.026 and AoA = 0°.

Number of grid cells, NS solution					
	100	200	400	600	800
C_D	0.4303	0.4222	0.4110	0.3956	0.3994

Table 5
Magnitudes of C_D for different Courant numbers at Mach = 2, Kn = 0.026 and AoA = 0°.

Values of Courant number			
	0.1	0.3	0.5
C_D	0.3992	0.3992	0.3989

pressure distribution coefficient for 5 test cases is the same. But if we concentrate on the slip velocity, we could see considerable differences. However, the solutions of 600 and 800 cells are almost close to each other. Table 4 shows the value of the drag coefficient on the airfoil surface for all test cases. The values show that C_D is approximately constant when we increase the number of grid points from 600 to 800. As a result, we do all NS simulations using the structured C-type grid with 600 cells on the airfoil surface.

We also performed three runs using different Courant numbers to confirm the independence of our simulations from the current number. We do these runs at Kn = 0.026 and zero angle of attack with values of 0.5, 0.3 and 0.1 for the Courant number. Table 5 shows C_D for three Courant numbers. According to the values reported in the Table, we can justify that our simulations are independent from the Courant number. Table 6 also provides a summary of the simulation setup for the DSMC and NS solvers for both the sub/supersonic test cases. The values chosen for subsonic case are selected after careful independency test cases.

3.2. Validation

3.2.1. Comparison with the experimental results

In this section, we compare the density and velocity field around our simulated test case with the experimental and computational data reported at Kn = 0.026, Mach = 2 and Kn = 0.014, Mach = 0.8, $\alpha = 0$ in Refs. [5,6]. All DSMC solutions reported in the rest of this paper are obtained using the SBT scheme. Fig. 5 shows solutions of the DSMC and NS equations subject to slip/jump boundary condition, and experimental contours [5,6] for the supersonic test case. The figure shows suitable agreement between the DSMC solution and NS solution subject to the slip/jump BC's and experimental data. This observation confirms the suitability of using the NS equation subject to the first order slip/jump boundary

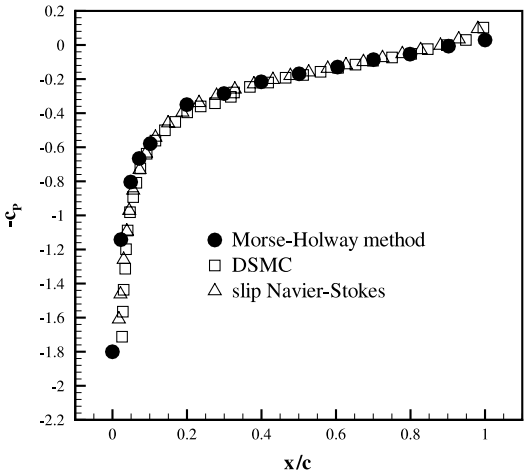

Fig. 6. Comparison of the average of upper and lower surface pressure distributions between different computational approaches at Mach $= 2$, Kn $= 0.026$ and $\alpha = 10°$.

conditions in the early slip regime in supersonic flow. The main benefit of using an NS solver is lower computational cost, i.e., for the current test case, computational time of the NS solver is around 12 h while that of DSMC is around 24 h.

Pressure coefficient distribution (C_p) is shown for the same Kn and Mach numbers but at $\alpha = 10°$ in Fig. 6. In this figure, the solution of DSMC and NS equations subject to slip/jump BC's are compared with the solution obtained from the Morse–Holway model [8]. The values presented in this figure are averages of C_p on the upper and lower surfaces of the airfoil. There is excellent agreement between the current results and that of Ref. [8], however, the NS solution predicts a lower value for C_p than others at the leading edge of the airfoil. This may be due to the effect of increase in the local Kn number near the leading edge. For the subsonic regime, we compare the velocity field contours with that of Ref. [9]. Fig. 7 shows the normalized velocity (V/V_∞) field around the airfoil at Kn $= 0.014$ and Mach $= 0.8$. The figure shows the agreement between DSMC and NS subject with slip/jump BC's is not as well as the agreement observed in supersonic case, i.e., Fig. 5.

3.3. Discussion on the pressure and velocity distributions

Fig. 8 illustrates the C_P distribution at three Knudsen numbers for both DSMC and NS slip calculations at $\alpha = 0°$. As is seen in the figure, at Kn $= 0.026$ where flow is in the slip regime, the results

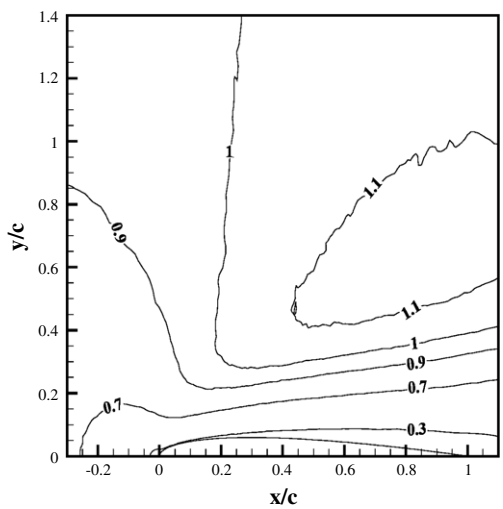

(a) DSMC.

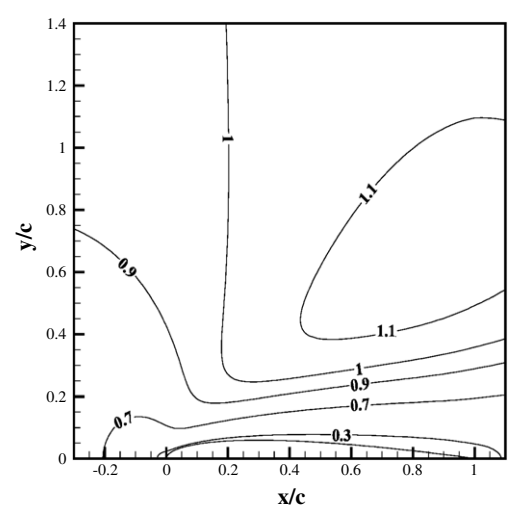

(b) NS with slip/jump BC's.

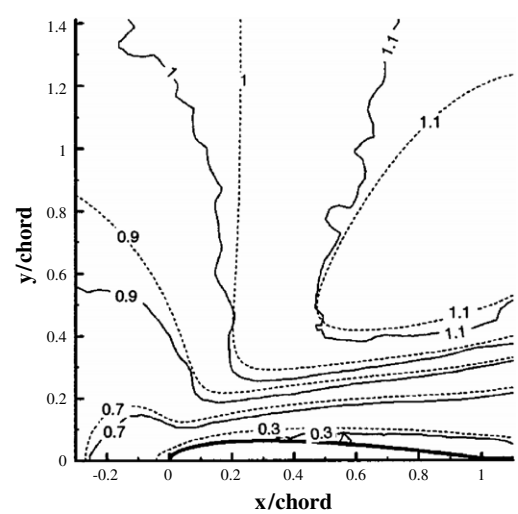

(c) Solution of Ref. [9], (solid line: DSMC, dashed line: NS).

Fig. 7. Comparison of the normalized velocity field from the current DSMC and NS solutions with the DSMC and NS solutions reported in Ref. [9], Mach $= 0.8$, Kn $= 0.014$, $\alpha = 0°$.

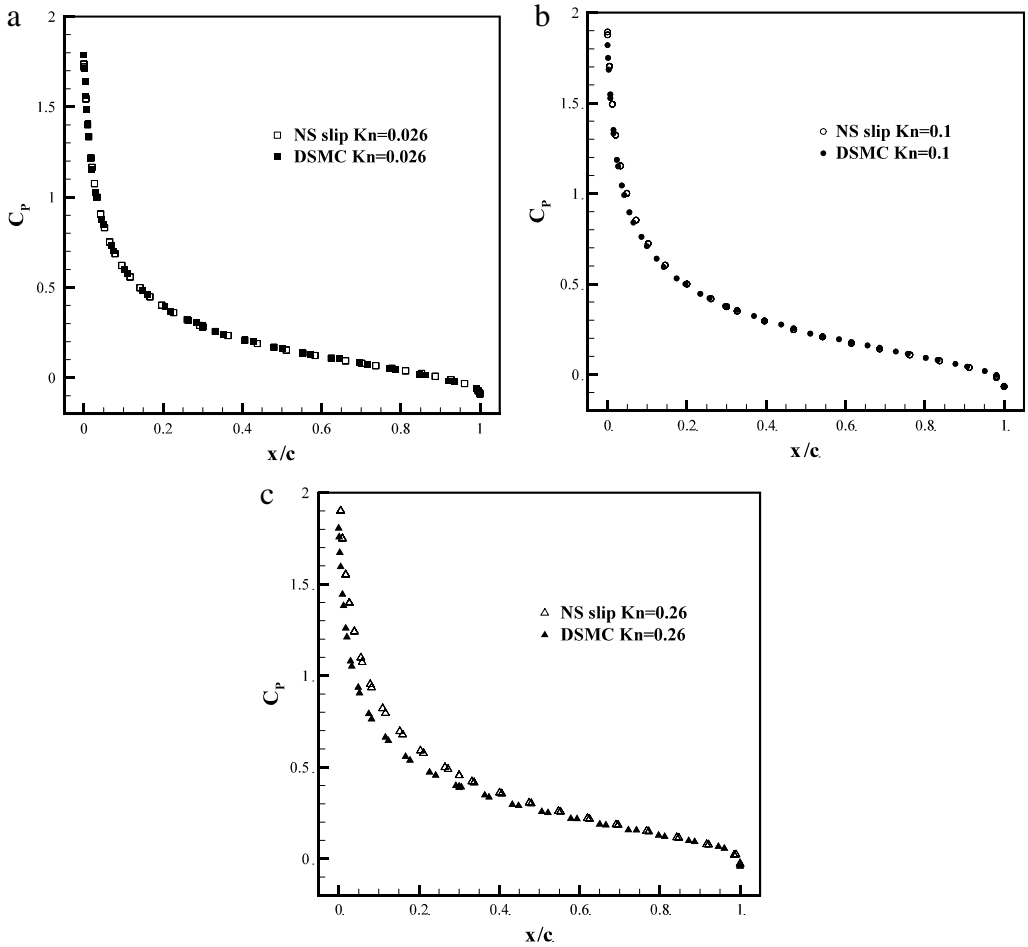

Fig. 8. Comparison of surface pressure distributions on the upper surface of the airfoil at three Knudsen numbers at Mach $= 2$, $\alpha = 0°$ (a) Kn $= 0.026$ (b) Kn $= 0.1$ (c) Kn $= 0.26$.

Table 6
Summary of simulation set-up for sub/supersonic test cases.

Flow regime	*Solver*	*Number of cells*	*Time step (DSMC) and (Courant No.)*	*Upstream boundary size*	*Downstream boundary size (In terms of c)*	*Particle per cell (DSMC)*	*Sample size (DSMC)*
	DSMC	312,900	6×10^{-8}	20	20	8	600,000
Subsonic	*NS*	132,000	6×10^{-8} (0.3)	30	30	–	–
	DSMC	145,500	3×10^{-7}	3	6	4	600,000
Supersonic	*NS*	145,500	3×10^{-7} (0.3)	3	6	–	–

for the NS with slip BC and DSMC are the same and this agreement remains up to Kn $= 0.1$, but this is correct only at zero angle of attack. At Kn $= 0.26$, where the flow is in transition regime, the results of two approaches are quite different, i.e., see Fig. 8(c), where NS equations predicts $C_P = 2.1$ at the leading edge of the airfoil while DSMC prediction is 1.8.

Fig. 9 shows the pressure coefficient and normalized slip velocity distribution over the airfoil at Mach $= 0.8$ and Kn $= 0.014$. Unlike the supersonic case and similar to Fig. 7, a disagreement is observed between the continuum and molecular solutions even in the early slip regime. This disagreement is due to the transonic nature ($0.8 <$ Mach < 1.2) of the considered test case, where the deviation from the equilibrium is intensified compared to the pure subsonic or supersonic condition.

Fig. 10 indicates the effect of increasing the Kn number on the pressure distribution coefficient and slip velocity. In Fig. 10, the DSMC results in three Kn numbers are shown at $\alpha = 20°$. Frame 10(a) shows that C_p for three cases are the same on the upper surface while C_p increases on the lower surface with the increase of the Knudsen number. As Kn number increases, the initial kinetic energy of the gas is converted to higher viscous forces as well as higher pressure magnitudes. On the other hand, if the airfoil had an angle of attack against the flow, the stagnation point will be located on the lower surface of the airfoil, so velocity is more affected by the viscous forces, which becomes stronger as Kn increases. Meanwhile, upper surface of the airfoil is less affected by the viscous force because velocity is higher there; therefore, velocity and pressure are somehow less dependent on the viscosity on the upper surface. Therefore, C_p is almost constant on the upper surface. As Fig. 10(b) shows, the increase in the slip velocity is higher on the upper surface of the airfoil. The flow is more rarefied on the upper surface, i.e., there are less number of particles there. Therefore, the increase in slip velocity at higher Kn number is attributed to a less number of particles, which subsequently do not reach into an equilibrium state with the surface.

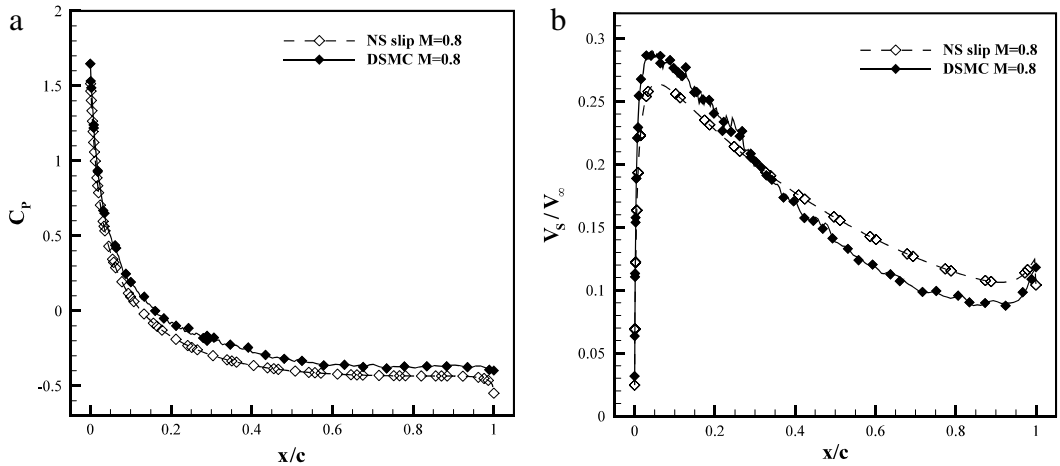

Fig. 9. Comparison of (a) surface pressure distributions and (b) normalized slip velocity at Mach = 0.8, Kn = 0.014 and $\alpha = 0°$.

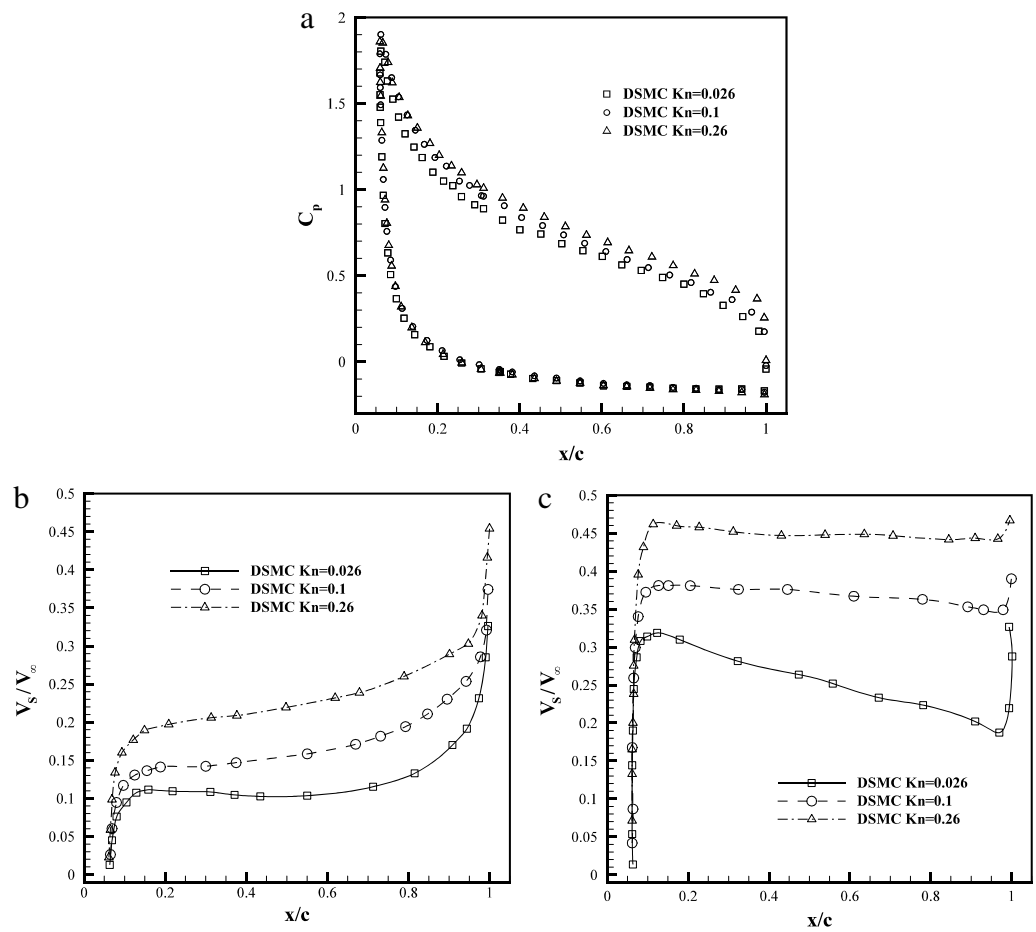

Fig. 10. Effect of Knudsen number on the (a) pressure coefficient, (b) slip velocity distributions at upper surface, (c) slip velocity distributions at lower surface, Mach = 2, $\alpha = 20°$.

Table 7
Shock position from the airfoil leading edge at different Knudsen numbers, DSMC solution, (Mach = 2, $\alpha = 0°$).

Kn number	0.026	0.10	0.26
Shock position ($-x/c$)	0.23	0.61	1.30

Fig. 11 shows the pressure coefficient along the stagnation line ahead of the airfoil at $\alpha = 0°$ and from both of the NS and DSMC solvers at 2 Kn number flows. This figure illustrates the starting point of the shock wave. As Kn number increases, the location of the shock moves farther from the airfoil, see Table 7. In fact, high viscous forces make the shock wave wider and more diffusive. The figure shows that NS solution predicts less diffusive and thinner shock compared to the DSMC solution, however, the post-shock properties are almost independent from the solver. Additionally, stagnation pressure slightly changes with the Kn number increase. Table 7 shows the shock wave location at different Kn numbers at $\alpha = 0°$ and DSMC solution. We take the location of the shock wave

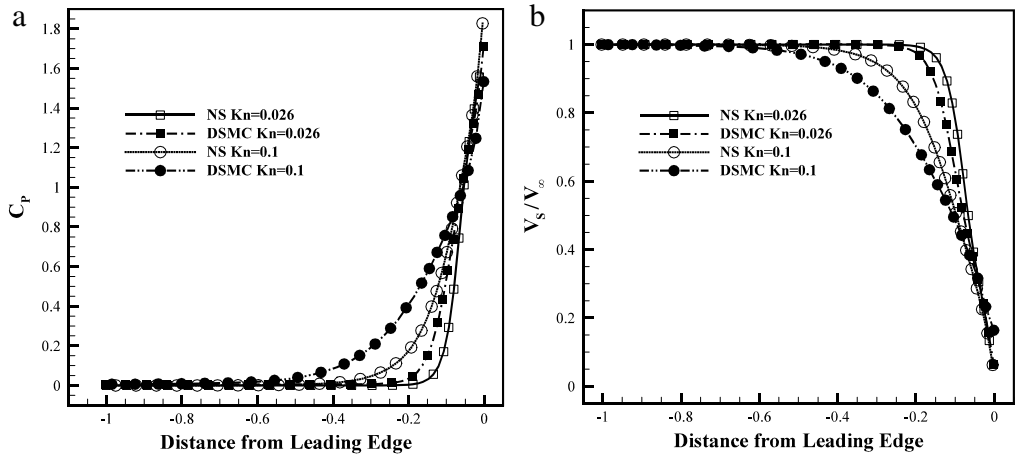

Fig. 11. (a) Pressure coefficient distribution and (b) normalized velocity on the stagnation line of the airfoil, Mach = 2, $\alpha = 0°$.

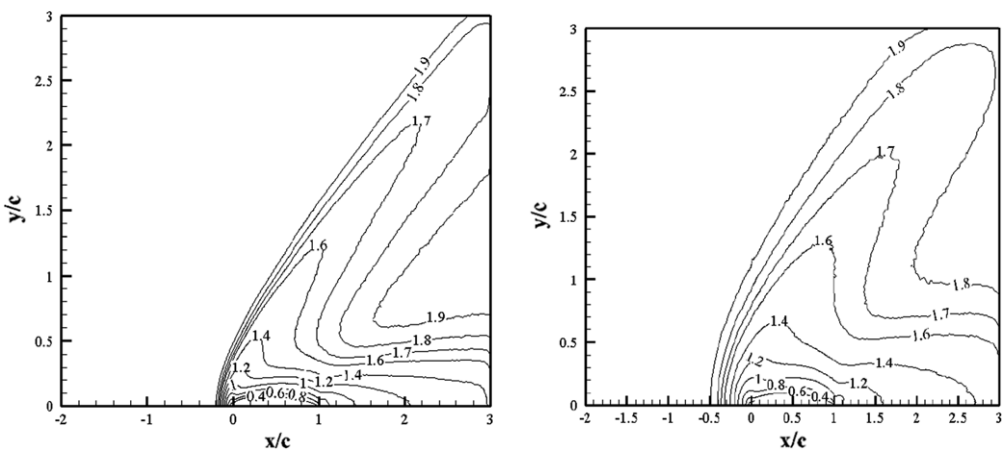

(a) Kn = 0.026.

(b) Kn = 0.1.

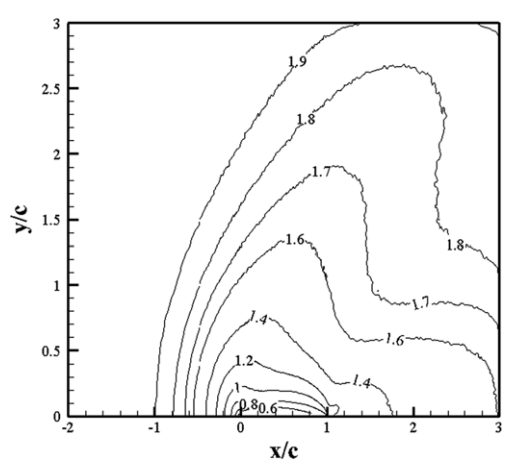

(c) Kn = 0.26.

Fig. 12. Mach number contour from DSMC solution at three different Kn numbers at Mach = 2, $\alpha = 0°$.

where the flow properties start dropping below 0.99 of the free stream properties values.

3.4. Mach number behavior at supersonic and subsonic regimes

Fig. 12 shows the Mach number contours at three different Kn number cases at $\alpha = 0°$. The figure indicates the dependency of the shock's shape and curvature on the Kn number. At higher Kn numbers, the shock is transformed into a series of diffusive waves extending toward the flow inlet. Additionally, shock is more curved at higher rarefaction regimes. At lower Kn number, the density of the flow is higher and if velocity remains constant, free stream has greater total kinetic energy at lower Kn number. Greater kinetic energy forces the shock waves to have sharp shape and locates it at the nearest position to the leading edge.

Fig. 13 shows the Mach number contours around the airfoil for subsonic case (Mach = 0.8) at Kn = 0.014 results. Frame (a) shows the Mach number contours from DSMC simulation at

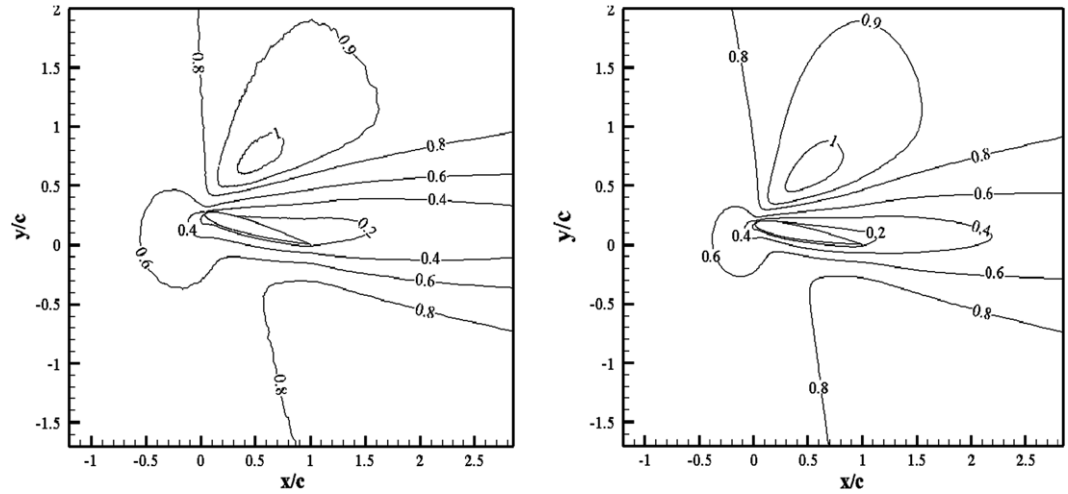

(a) DSMC. (b) Slip/jump NS.

Fig. 13. Mach number contours around the airfoil at $M = 0.8$ and Kn $= 0.014$ (a) DSMC, $\alpha = 15^\circ$, (b) slip NS, $\alpha = 10^\circ$.

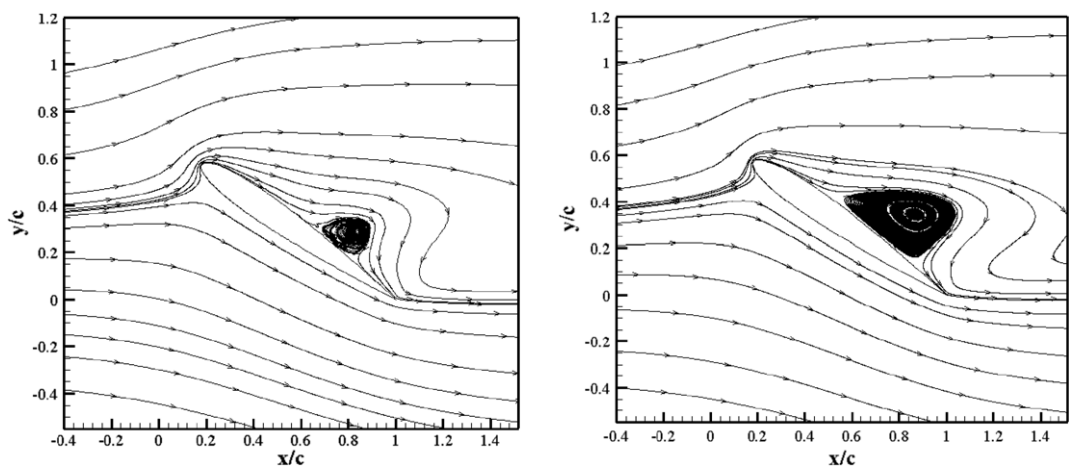

(a) DSMC, $M = 0.8$. (b) NS slip, $M = 0.8$.

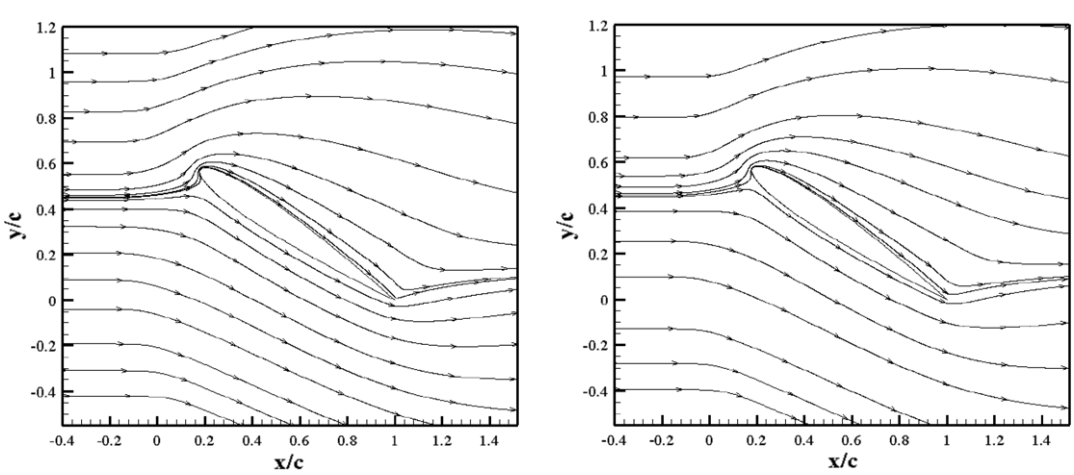

(c) DSMC, $M = 2$. (d) NS slip, $M = 2$.

Fig. 14. Streamline at different Mach numbers and $\alpha = 35^\circ$ from the DSMC and slip/jump NS solution at the slip regime.

AoA $= 15^\circ$. Frame (b) indicates the same contours from the NS with slip/jump solution at AoA $= 10^\circ$. Angles of attack are different because the NS solution did not predict supersonic region at AoA $= 10^\circ$. Region of supersonic flow is limited to far distance from the airfoil surface due to thick boundary layer formation on the airfoil. Once the flow field around the airfoil consists of both the sub and supersonic regions, the flow is called transonic. In transonic regime, flow is highly non-linear and non-equilibrium effects are magnified [25].

In Fig. 14, a comparison between subsonic and supersonic flow regimes at slip regime and at the same angle of attack is provided. This figure shows that separation on the airfoil surface is observed

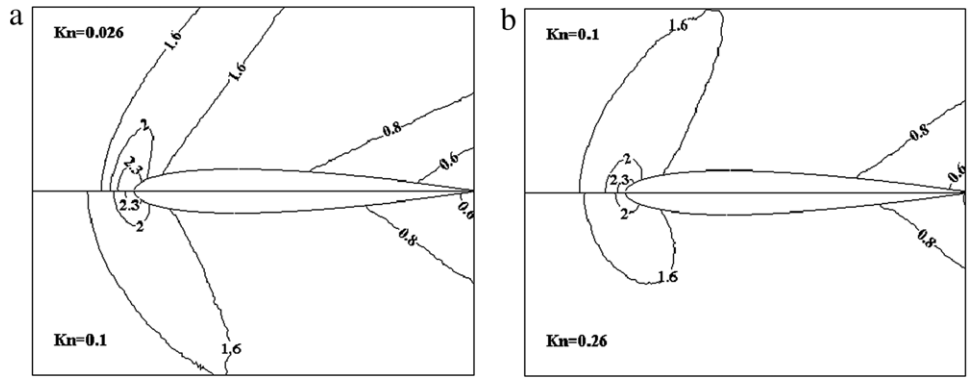

Fig. 15. Comparison of normalized density field contours at three Kn numbers, Mach = 2, $\alpha = 0°$.

from both the DSMC and NS solutions at the subsonic flow but separation does not exist for supersonic flow. For supersonic flow, our simulation showed that no separation occurs even at higher angles of attack up to 55°. This can be related to the higher total kinetic energy of the freestream flow at $M = 2$. At $M = 0.8$, slip/jump NS solution predicts a larger separation zone in comparison with the DSMC solution. Additionally, in comparison with the DSMC solution, NS prediction for the starting point of separation is located closer to the leading edge.

3.5. Density and shear stress at supersonic flow

Contours of the normalized density field (ρ/ρ_∞) at three Kn number are illustrated in Fig. 15. The figure shows that the density variations decreases when Kn number increases. This result is in contrast with results from Ref. [10] for subsonic regime. Our results confirm that the compressibility of flow decrease when the Kn number increases.

Fig. 16 indicates the wall shear stress on the airfoil surface at three Kn number and at AoA = 45 from the DSMC results. For all three Kn numbers, there are large amounts of shear stress at the leading edge at the upper surface of the airfoil. Then, shear stress sharply decreases. By increasing Kn number, smaller values of shear stress is observed. This decrease could be attributed to lower number of particle–surface interactions.

3.6. Discussion on aerodynamics characteristics of airfoil at the sup/subsonic regimes

Fig. 17 shows the full aerodynamic characteristics of NACA 0012 airfoil under rarefied conditions. The lift and drag coefficients (C_L and C_D) calculated for current simulations are plotted in Fig. 17(a)–(c). Fig. 17(a) shows the values from both the DSMC and NS solutions with slip/jump BC's at Kn = 0.026. As expected, the DSMC and NS results are in full agreement with each other in this Kn number. In this figure, the DSMC results are plotted until AoA = 55° but NS results are plotted until 45°, because based on the local rarefaction effects on the upper surface of the airfoil, the flow largely departs from equilibrium condition and NS equations fail to simulate the flow field at AoA > 45°. The lift slope is 2 in this Kn number and the drag coefficient is about 0.4 for very small angle of attack.

Fig. 17(b) shows the results when Kn = 0.1. In this case, NS solutions show a deviation from the DSMC results specially for C_D and C_L near the stall point. NS solution predicts bigger drag coefficient and smaller angle of attack for stall point. Here, the lift slope is 2.09 and the drag coefficient is approximately 0.6 for small angle of attack.

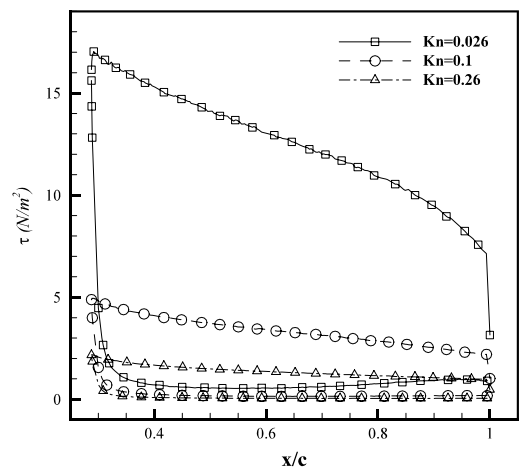

Fig. 16. Wall shear stress on the airfoil surface at different Kn numbers, Mach = 2, $\alpha = 45°$, DSMC calculations.

Fig. 17(c) demonstrates the results at Kn = 0.26. Even though at this Kn number the NS solution is not valid, it is observed that the NS solution for the lift coefficient is in suitable agreement with the DSMC solution. Here, lift slope increases to 2.16 for this case and the drag coefficient is less than 0.8 for small angle of attack.

Fig. 17(d) and (e) demonstrate the lift and drag coefficients at three different Kn numbers in comparison with the linearized theory,

$$C_L = 4\alpha \Big/ \sqrt{M_\infty^2 - 1} \tag{24}$$

$$C_D = 4\alpha^2 \Big/ \sqrt{M_\infty^2 - 1} + 4\left(\frac{t}{c}\right)^2 \Big/ \sqrt{M_\infty^2 - 1}. \tag{25}$$

As Fig. 17(d) shows, C_L has no visible change with increasing in the Kn number. Shown in Fig. 17(e) is the calculated drag coefficient at different Kn numbers. The results illustrate that C_D increases with increase in the Kn number. At small angles of attack up to $\alpha = 10°$, the lift coefficient at different Kn numbers agrees suitably with the linearized theory while the drag coefficient calculated based on the linearized theory deviates from the simulation results. This shows the linearized theory does not predict an accurate value for C_D due to ignorance of viscous forces.

Fig. 17(f) indicates the airfoil drag polar, that is, (C_L/C_D). For Kn number of 0.026 and 0.1, results for both DSMC and NS are shown, but at Kn = 0.26, only DSMC values are shown. The maximum value of curves occurs at $\alpha = 25°$ in all 3 investigated cases. By

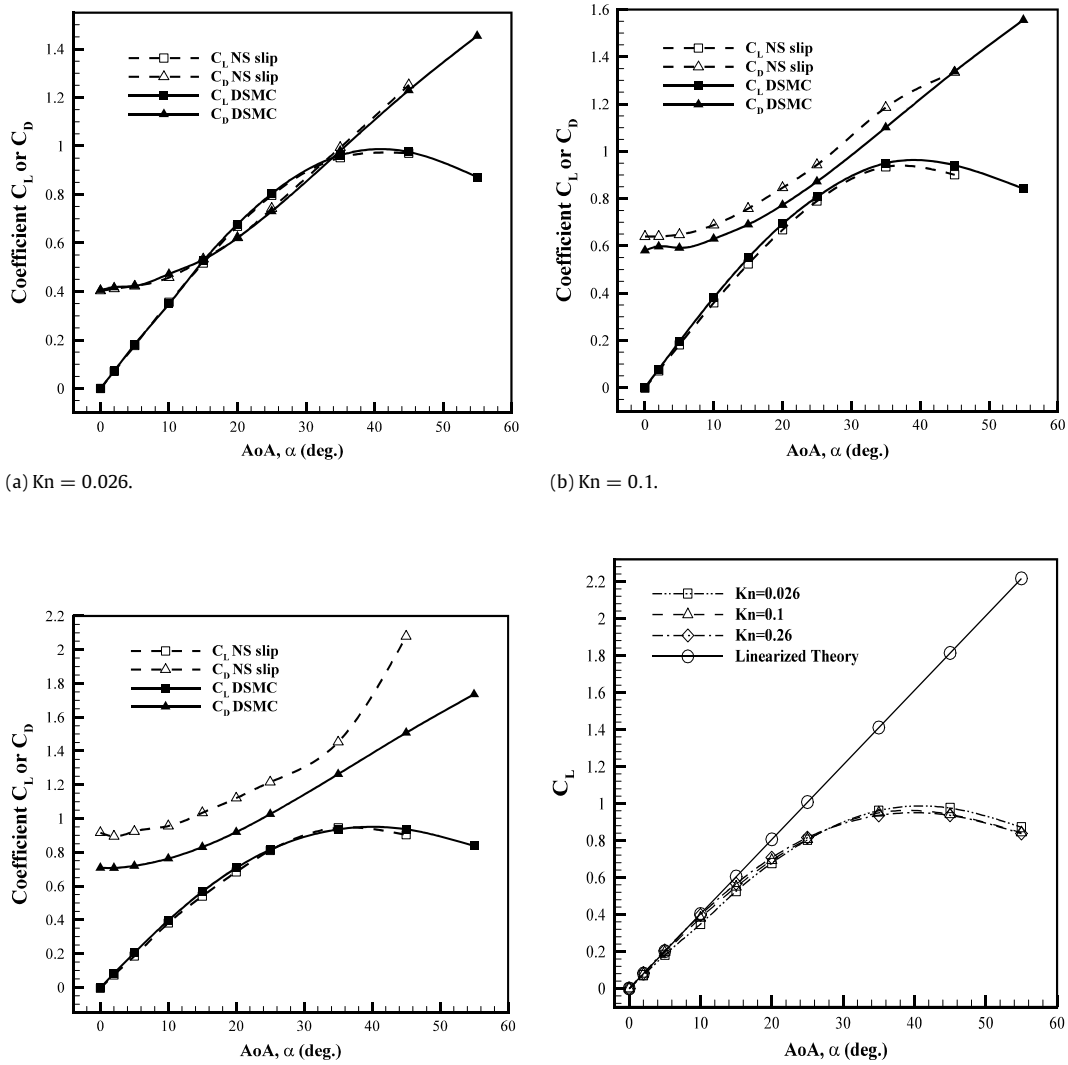

(a) Kn = 0.026.

(b) Kn = 0.1.

(c) Kn = 0.26.

(d) C_L comparison.

Fig. 17. Aerodynamics performance of the airfoil at supersonic regime.

increasing the Kn number, the value of C_L/C_D decreases. Looking at Fig. 17(d) and (e), with increasing Kn number, drag coefficient increases, but the lift coefficient approximately remains the same. Decreasing the Kn number is beneficial as we have a higher C_L/C_D at the same angle of attack.

Fig. 17(g) shows the drag coefficient at $\alpha = 0°$ and lift slope at different Kn numbers. This figure shows that the lift slope is lower than its linearized value at small Kn number flows but it increases as Kn increases. This observation is consistent with the conclusions reported in Ref. [11] for flat plate airfoil at rarefied subsonic regimes. The figure shows that drag force is higher than its linearized value and it increases as Kn number increases.

Fig. 18(a) and (b) show the comparison between C_L and C_D from the numerical subsonic simulation at Kn = 0.014 and Mach = 0.8 with the linearized theory. Frame 18(a) shows that the NS with slip/jump BC's overpredict the lift coefficient in comparison with the DSMC solution. Linearized theory overpredicts the numerical solution considerably. About the drag coefficient, the trend of the DSMC and NS solutions are similar to the linearized theory; however, similar to the C_L, there is a substantial difference between the DSMC and NS solutions with the linearized theory. In fact, it is well-known that the linearized theory is invalid for transonic regime ($0.8 < \text{Mach} < 1.2$) and also it ignores the viscous forces; therefore, inconsistency between the linearized theory and numerical solutions is expected at transonic regime. Fig. 18(c) shows that the maximum value of C_L/C_D occurs between 20°–25°. Therefore, it is concluded that airfoils utilized in micro scale devices could operate suitably at higher angles of attacks compared to macro-scale applications.

To further justify the difference between the DSMC and NS solutions, we computed the Knudsen number based on the gradient local length (GLL) of the flow properties. This parameter is defined as:

$$\text{Kn}_{GLL\emptyset} = \frac{\lambda}{\phi} |\nabla \emptyset| \tag{26}$$

where ϕ is an arbitrary flow parameter and $\text{Kn}_{GLL} = \text{Max}(\text{Kn}_{GLL,\rho}, \text{Kn}_{GLL,|V|}, \text{Kn}_{GLL,T})$. Comparison between the DSMC and NS results showed that the continuum approach broke down where Kn_{GLL} exceeds 0.05 [28]. Fig. 19 shows this parameter around the airfoil at AoA = 35° and Mach = 0.8. The figure indicates that Kn_{GLL} exceeds the threshold value at the leading edge and trailing edge

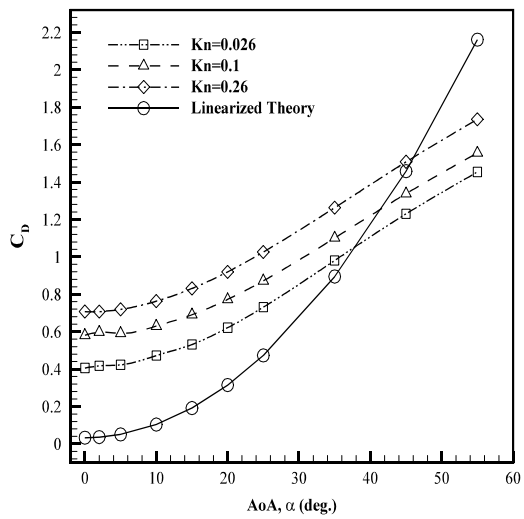

(e) C_D comparison.

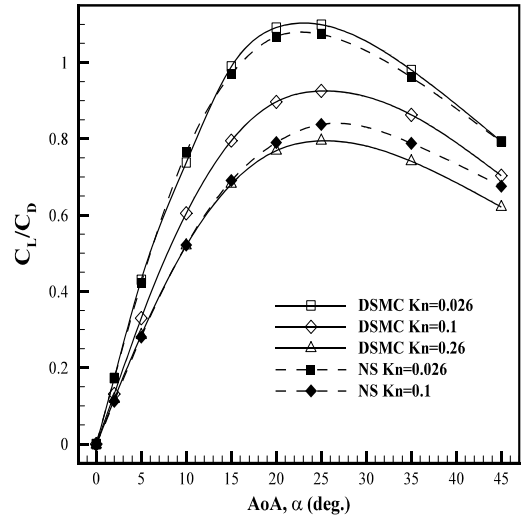

(f) Drag polar.

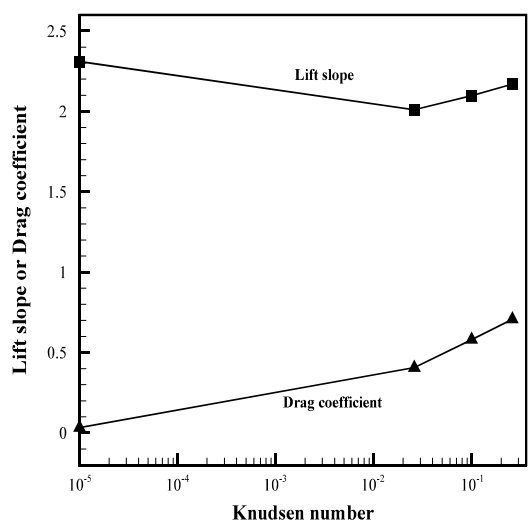

(g) Lift slop and drag coefficient at $\alpha = 0°$.

Fig. 17. (*continued*)

of the airfoil. Therefore, the NS results broke down at this Mach number and relatively high angle of attacks.

For more efficient and less expensive simulations of rarefied flow around the airfoil, one could employ a hybrid NS/DSMC technique where the DSMC solution is limited to the non-equilibrium regions, i.e., where $\mathrm{Kn}_{GLL} > 0.05$, while the near-equilibrium region could be treated with the NS solver. For more details on a typical hybrid NS/DSMC technique, see Refs. [13,15].

4. Conclusion

The aerodynamics of NACA 0012 airfoil at sub/supersonic air stream was investigated using both the continuum and particles approaches at three Kn numbers over a wide range of flow angle of attack. Our study showed that NS equations with slip/jump BC's are valid at slip regime, especially for C_p and C_L. Density field and pressure coefficient distribution of particle and continuum approaches in the slip regime were compared with the available experimental data and good agreement was observed. Comparison between C_p at different Kn numbers shows that the C_p at lower surface of the airfoil increases with increasing the Kn number while it is constant on the upper surface. Meanwhile, the shock shape and curvature vary with the variation of the Kn number. The compressibility of the air stream around the airfoil decreases with the increase of the Kn number. At low Kn number and small angle of attacks, C_L values agree with the linearized theory; however, as Kn number increases, the deviation is observable. With the increase in the Kn number in supersonic regime, the lift coefficient is approximately constant, while drag coefficient increases. The stall point has not any visible change with increasing of the Kn number. The maximum ratio of lift to drag occurs at an angle of attack of 25° for supersonic regime.

Acknowledgments

The authors would like to acknowledge the financial supports provided by the Faculty of Engineering, Ferdowsi University of Mashhad under Grant No. 25270. The last author S.S. would like to

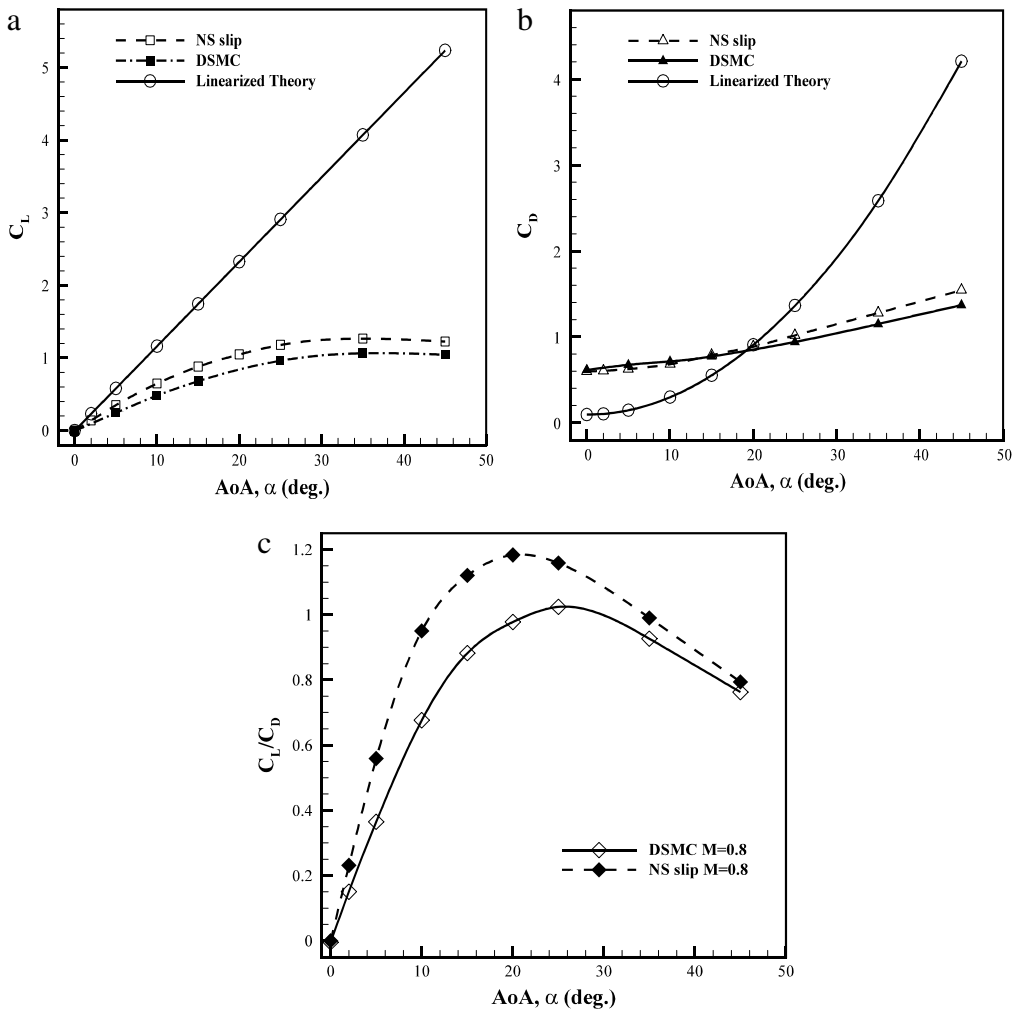

Fig. 18. Aerodynamics coefficients and performance of the airfoil at subsonic regime.

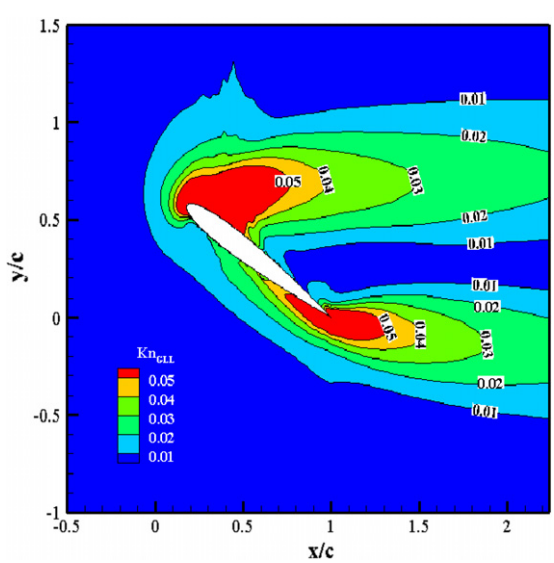

Fig. 19. Contours of Kn_{GLL} around the airfoil at Mach = 0.8, $\alpha = 35°$.

acknowledge the financial support provided by the NSF of Bulgaria under Grant No. DUNK 1/3-2009.

References

[1] S.A. Schaaf, P.L. Chambre, Flow of Rarefied Gases, Princeton University Press, USA, 1961.

[2] G. Karniadakis, A. Beskok, N. Aluru, Microflows and Nanoflows: Fundamentals and Simulation, Springer-Verlag, New York, 2005.

[3] C.M. Ho, Y.C. Tai, Micro-electro-mechanical-system (MEMS) and fluid flows, Annu. Rev. Fluid Mech. 30 (1998) 579–612.

[4] G.A. Bird, Molecular Gas Dynamics, Clarendon Press, Oxford, 1976.

[5] J. Allegre, M. Raffin, J.C. Lengrand, Experimental flow fields around NACA 0012 airfoils located in subsonic and supersonic rarefied air streams, in: M.O. Bristeau, R. Glowinski, J. Periaux, H. Viviand (Eds.), Numerical Simulation of Compressible Navier–Stokes Flows, Friedr.Vieweg and Sohn, Braunschweig, Germany, 1985, pp. 59–68.

[6] J. Allegre, M. Raffin, L. Gottesdient, Slip effect on supersonic flow fields around NACA 0012 airfoils, in: V. Boffi., C. Cercigani (Eds.), Rarefied Gas Dynamics 15, 1986, pp. 548–557.

[7] W. Hasse, Solution of the Navier–Stokes equations for sub and supersonic flows in rarefied gases, in: M.O. Bristeau, R. Glowinski, J. Periaux, H. Viviand (Eds.), Numerical Simulation of Compressible Navier–Stokes Flows, Friedr. Vieweg and Sohn, Braunschweig, Germany, 1985, pp. 139–157.

[8] J.Y. Yang, J.C. Huang, C.S. Wang, Non-oscillatory schemes for kinetic model equations for gases with internal energy states, AIAA J. 34 (1996) 2071–2081.

[9] J. Fan, I.D. Boyd, C.P. Cai, Computation of rarefied gas flows around a NACA 0012 airfoil, AIAA J. 39 (2001) 618–625.

[10] Q. Sun, I.D. Boyd, Flat-plate aerodynamics at very low Reynolds number, J. Fluid Mech. 502 (2004) 199–206.

[11] G. Zuppardi, G. Visone, R. Votta, A. Schettino, Analysis of aerodynamic performances of experimental flying test bed in high-altitude flight, Proc. Inst. Mech. Eng. G 225 (2011) 247–258.

[12] H. Akhlaghi, M. Balaj, E. Roohi, Hydrodynamic behaviour of micro/nanoscale poiseuille flow under thermal creep condition, Appl. Phys. Lett. 103 (7) (2013) 073108.
[13] M. Darbandi, E. Roohi, A hybrid DSMC/Navier–Stokes frame to solve mixed rarefied and non-rarefied micro/nanoflows, Int. J. Numer. Methods Fluids 72 (9) (2013) 937–966.
[14] A. Mohammadzadeh, E. Roohi, H. Niazmand, A parallel DSMC investigation of monatomic/diatomic gas flows in micro/nano cavity, Numer. Heat Transfer A 63 (4) (2013) 305–325.
[15] M. Darbandi, E. Roohi, Applying a hybrid DSMC/Navier–Stokes frame to explore the effect of splitter plates in micro/nano propulsion systems, Sensors Actuators A 189 (2013) 409–419.
[16] J.D. Anderson, Hypersonic and High Temperature Gas Dynamics, AIAA Press, 2007.
[17] OpenFOAM: The Open Source CFD Toolbox, User Guide, Version 2.01, OpenFOAM Foundation 2011.
[18] C.J. Greenshields, H.G. Weller, L. Gasparini, J.M. Reese, Implementation of semi-discrete, non-staggered central schemes in a collocated, polyhedral, finite volume framework, for high-speed viscous flows, Internat. J. Numer. Methods Fluids 63 (2010) 1–21.
[19] A. Kurganov, E. Tadmor, New high-resolution central schemes for nonlinear conservation laws and convection–diffusion equations, J. Comput. Phys. 160 (2001) 241–282.
[20] A. Kurganov, S. Noelle, G. Petrova, Semi-discrete central-upwind schemes for hyperbolic conservation laws and Hamilton–Jacobi equations, SIAM J. Sci. Comput. 23 (2001) 707–740.
[21] F. Sharipov, Data on the velocity slip and temperature jump on a gas–solid interface, J. Phys. Chem. Ref. Data. 40 (2) (2011) 023101.
[22] T. Scanlon, E. Roohi, C. White, M. Darbandi, J. Reese, An open source Parallel DSMC code for rarefied gas flows in arbitrary geometries, Comput. & Fluids 39 (10) (2010) 2078–2089.
[23] S. Stefanov, On DSMC calculations of rarefied gas flows with small number of particles in cells, SIAM J. Sci. Comput. 33 (2011) 677–702.
[24] G.B. Macpherson, N. Nordin, H.G. Weller, Particle tracking in unstructured, arbitrary polyhedral meshes for use in CFD and molecular dynamics, Commun. Numer. Methods Eng. 25 (3) (2009) 263–273.
[25] J. Anderson, Fundamentals of Aerodynamics, in: McGraw Hill Series in Aeronautical and Aerospace Engineering, 2010.
[26] W.W. Liou, Y. Fang, Microfluid Mechanics: Principles and Modelling, McGraw-Hill, London, 2006.
[27] A. Amiri, E. Roohi, H. Niazmand, S. Stefanov, DSMC simulation of low Knudsen micro/nano flows using small number of particles per cell, J. Heat Transfer 135 (10) (2013) 101008.
[28] I. Boyd, G. Chen, G.V. Candler, Predicting failure of the continuum fluid equations in transitional hypersonic flows, Phys. Fluids 7 (1995) 210–219.